Supplemental Document

Optics Letters

Development and characterization of a disposable submillimeter fiber optic Raman needle probe for enhancing real-time *in vivo* deep tissue and biofluids Raman measurements: supplement

Chi Shu,[1] Wei Zheng,[1] Zhuo Wang,[2] Changyuan Yu,[2] and Zhiwei Huang[1,*]

[1] *Optical Bioimaging Laboratory, Department of Biomedical Engineering, Faculty of Engineering, National University of Singapore, Singapore 117576, Singapore*
[2] *Photonics Research Center, Department of Electronic and Information Engineering, The Hong Kong Polytechnic University, Hong Kong, 999077, China*
[*] *Corresponding author: biehzw@nus.edu.sg*

Supplement DOI: https://doi.org/10.6084/m9.figshare.16663483

Parent Article DOI: https://doi.org/10.1364/OL.438713

Development and characterization of disposable sub-millimeter fiberoptic Raman needle probe for enhancing real-time in vivo deep tissue and biofluids Raman measurements: supplemental document

CHI SHU,[1] WEI ZHENG,[1] ZHUO WANG,[2] CHANGYUAN YU,[2] AND ZHIWEI HUANG[1,*]

[1]*Optical Bioimaging Laboratory, Department of Biomedical Engineering, Faculty of Engineering, National University of Singapore, Singapore 117576*
[2]*Photonics Research Center, Department of Electronic and Information Engineering, The Hong Kong Polytechnic University, Hong Kong, China, 999077*
**Corresponding author: biehzw@nus.edu.sg*

This document provides supplementary information for "Development and characterization of disposable sub-millimeter fiberoptic Raman needle probe for enhancing real-time in vivo deep tissue and biofluids Raman measurements", including: **(S1)** Monte Carlo simulations of fiberoptic Raman needle probe, and the customized Raman system description, **(S2)** Characterization of fiber silica Raman and fluorescence background versus fiber probe length and integration time, and **(S3)** Structured background subtraction algorithm development for eliminating fiber silica Raman/fluorescence and tissue autofluorescence background.

S1. Monte Carlo Simulations of fiberoptic Raman needle probe and the customized Raman system description

We examine the Raman performance of the fiberoptic Raman needle probe in scattering media (e.g., brain tissue) by using the ray tracing matrix and Monte Carlo (MC) simulation methods [1,2]. The Raman photon excitation and collection ability of the tapered Raman needle probe compared to the flat Raman probe in brain tissue are further analyzed using MC simulations. Based on the ray tracing matrix calculation, the effective focal length of the tapered fiberoptic Raman needle probe is ~ 250 μm, and the focal spot diameter is ~280 μm. For MC modeling, the refraction indices of the fiber probe and tissue are set as 1.45 and 1.35, respectively. The optical properties (e.g., scattering coefficient μ_s; absorption coefficient μ_a; anisotropy factor g; refractive index n, and layer thickness) of the brain tissue model are extrapolated from Ref [3]: (i) For 785 nm light excitation wavelength: μ_s= 78 cm^{-1}, μ_a = 0.2 cm^{-1}, g = 0.9, and n =1.35, (ii) For 900 nm Stokes Raman photon collection, μ_s = 66 cm^{-1}, μ_a = 0.6 cm^{-1}, g =0.9, n =1.35.

Fig. S1 shows the MC simulation results of normalize Raman photons collected by the tapered semi-spherical lens Raman needle probe and the flat Raman probe in brain tissue model. The Raman needle probe tapered with a semi-spherical lens provides at least 2.2-fold higher in total Raman collection efficiency compared to the flat Raman probe. Further, the maximum tissue Raman signal can be picked up from the subsurface ~200 μm of the brain tissue with >85% of tissue Raman signal being collected from the tissue depth within 300 μm, confirming the ability of the unique tapered lens Raman needle probe design for near needle-tip signal detection.

The performance of the submillimeter fiberoptic Raman needle probe designed and fabricated is then evaluated using the customized Raman system where were reported

elsewhere [4,5]. Briefly, the fiberoptic Raman spectroscopy system consists of a 785 nm diode laser (maximum power: 600 mW, B&W TEK Inc.), a high throughput reflective imaging spectrograph (Acton LS-785 *f*/2, Princeton Instrument Inc.) equipped with an 830 g/mm gold-coated grating, a NIR-enhanced deep-depletion charge-coupled device (CCD) camera (PIXIS 400BR-eXcelon, Princeton Instrument Inc.), and a customized hand-held optical coupling module for excitation laser coupling, and Raman signal filtering and collection. The wavelength and wavenumber axis of the spectrometer is calibrated using mercury-argon lamps (HG-1 and AR-1, Ocean Optics Inc.) and 4-acetamidophenol (ASTM E1840 standard) in FP and HW regions, respectively. The system intensity response is then calibrated using a standard reference material (NIST 2241, National Institute of Standards and Technology) [6].

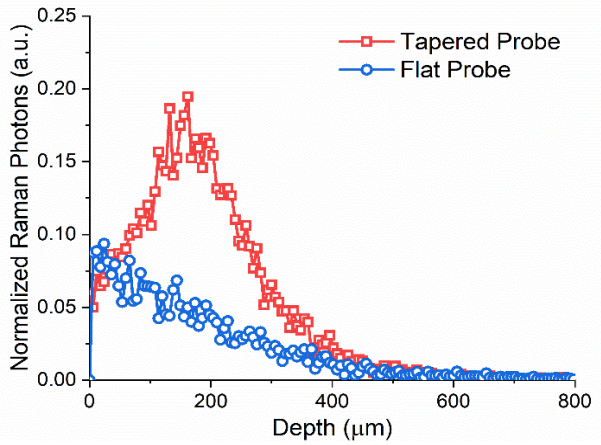

Fig. S1 Normalized Raman photons as a function of tissue depth in brain tissue collected by a semi-spherical tapered lens Raman needle probe (tapered probe) and a Raman probe with flat tip (flat probe) by using Monte Carlo simulations. For comparison purpose, the Raman photons collected by the Raman probes are normalized to the excitation photon number of $1x10^6$ in MC simulations.

S2. Characterization of fiber silica Raman and fluorescence background versus fiber probe length and integration time

The fiber silica Raman and fluorescence background signals of the fiberoptic Raman needle probes are characterized under different probe lengths and acquisition time. Fig. S2(a) show the example of mean maximum photon counts (e.g., 800 cm^{-1}) with ±1 standard deviation (SD) using the fiberoptic Raman needle probes with fiber lengths varying from 6.5 to 16 cm with 0.5 s integration time and 30 mW laser excitation power. Based on the fit function in Fig. S2(a), the fiber probe design can be up to 20 cm in fiber length under 0.5 s integration time and 30 mW laser excitation power before reaching the system saturation point (i.e., 65535 photon counts per pixel). Fig. S2(b) show the mean maximum photon counts (e.g., 800 cm^{-1}) with ±1 SD versus integration time of 0.1 to 1 s using a 10 cm fiberoptic Raman needle probe under 30 mW laser excitation power. The performance of all the fiberoptic needle Raman probes fabricated show a good linear relationship (r^2~1) with respect to both the fiber probe length and integration time, substantiating the robustness of the structured background subtraction algorithms developed (details refer to **section S3**) for pure tissue Raman spectra retrieval.

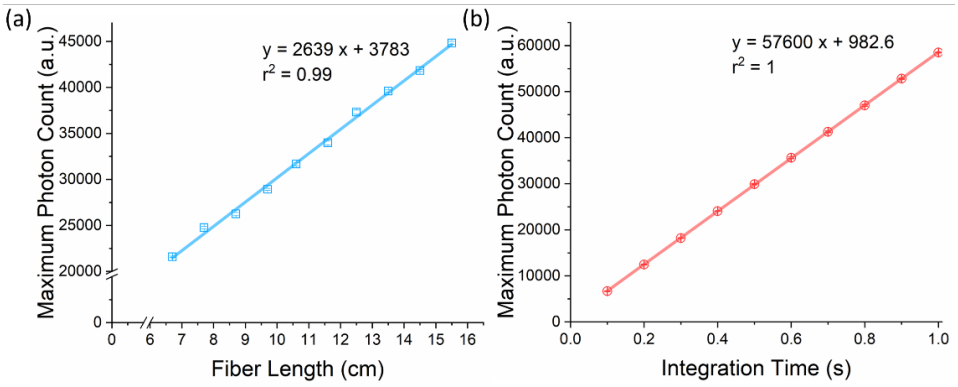

Fig. S2 (a) Mean maximum fiber background photon counts with ±1 standard deviation (SD) (e.g., 800 cm^{-1}) by using fiberoptic Raman needle probes under different fiber lengths (6.5 to 16 cm); (b) Mean maximum fiber background photon counts with ±1 SD (e.g., 800 cm^{-1}) versus different integration time of 0.1 to 1 s under a 10 cm fiberoptic Raman needle probe with 30 mW laser excitation power.

S3. Structured background subtraction algorithm development for eliminating interference of fiber silica Raman/ fluorescence and tissue autofluorescence background

Fig. S3 shows the flowchart of the structured background subtraction algorithm developed for eliminating the interference of fiber silica Raman/fluorescence background, as well as tissue autofluorescence (AF) background [7,8]. The method assumes that the measured tissue raw spectrum S_{raw} contains three parts: (i) The fiber Raman and fluorescence background S_{fiber} with the concentration c_{est}; (ii) The tissue AF background spectrum S_{auto}, which can be represented by a polynomial function, and (iii) pure tissue Raman spectrum S_{tissue}. During the data processing, the sample raw spectrum S_{raw} is loaded into the algorithm as the S_{input} together with the measured fiber silica Raman and fluorescence background spectrum S_{fiber}. Then the algorithm will iteratively estimate the interference concentration c_{est} of fiber background spectrum S_{fiber} in the raw sample spectrum S_{raw}. In each iteration, the interference concentration c_{est} together with tissue AF background S_{auto} are estimated by finding the optimized c_{est} and S_{auto}, which minimizes the function, $S_{raw} - c_{est}S_{fiber} - S_{auto}$, to be as small as possible, or to a certain preset value. Then, the fitted background spectrum is calculated as $S_{bg} = c_{est}S_{fiber} + S_{auto}$. The input spectrum S_{input} in the next iteration is then updated by comparing S_{input} and S_{bg}. All the features in the S_{input} exhibiting above the estimated background S_{bg} are considered as pure Raman signal and will be subtracted and replaced by the estimated background S_{bg}, while all the features in the S_{input} exhibiting below the estimated background S_{bg} are considered as unfitted spectrum which will be remained in S_{input}. The algorithm will converge after many rounds of iterations or until the change of the input spectrum S_{input} compared to the last iteration to be < 1 % or even a smaller value set. The pure tissue Raman spectrum is then calculated as $S_{tissue} = S_{raw} - c_{est}S_{fiber} - S_{auto}$ using the polynomial fitting functions, and the c_{est} is calculated in the last round of iterations.

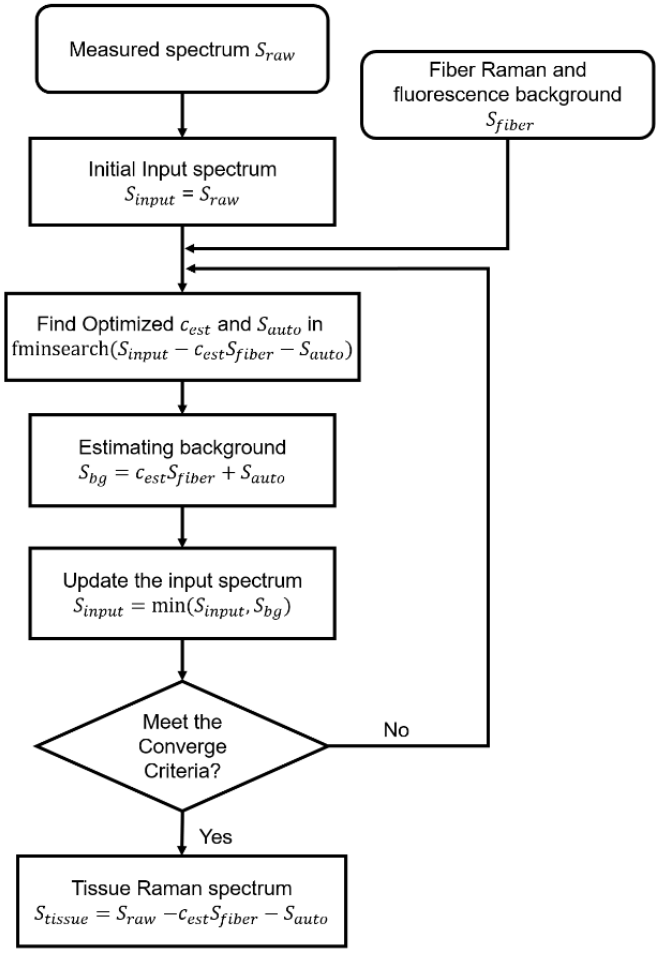

Fig. S3 Flowchart of the structured background subtraction algorithms developed for eliminating the interference of fiber silica Raman/fluorescence background and tissue autofluorescence (AF) background

References

1. J. Wang, M. S. Bergholt, W. Zheng, and Z. Huang, "Development of a beveled fiber-optic confocal Raman probe for enhancing in vivo epithelial tissue Raman measurements at endoscopy," Opt. Lett. **38**, 2321–2323 (2013).
2. J. Mo, W. Zheng, and Z. Huang, "Fiber-optic Raman probe couples ball lens for depth-selected Raman measurements of epithelial tissue," Biomed. Opt. Express **1**, 17–30 (2010).
3. J. D. Johansson, "Spectroscopic method for determination of the absorption coefficient in brain tissue," J. Biomed. Opt. **15**, 1–9 (2010).
4. K. Lin, W. Zheng, C. M. Lim, and Z. Huang, "Real-time In vivo Diagnosis of Nasopharyngeal Carcinoma Using Rapid Fiber-Optic Raman Spectroscopy," Theranostics **7**, 3517–3526 (2017).
5. K. Lin, J. Wang, W. Zheng, K. Y. Ho, M. Teh, K. G. Yeoh, and Z. Huang, "Rapid Fiber-optic Raman Spectroscopy for Real-Time In Vivo Detection of Gastric Intestinal Metaplasia during Clinical Gastroscopy," Cancer Prev. Res. **9**, 476–483

(2016).
6. S. Choquette, E. S Etz, W. Hurst, D. H Blackburn, and S. D Leigh, *Relative Intensity Correction of Raman Spectrometers: NIST SRMs 2241 Through 2243 for 785 Nm, 532 Nm, and 488 Nm/514.5 Nm Excitation* (2007), Vol. 61.
7. B. D. Beier and A. J. Berger, "Method for automated background subtraction from Raman spectra containing known contaminants," Analyst **134**, 1198–1202 (2009).
8. Z. Huang, A. McWilliams, S. Lam, J. English, D. I. McLean, H. Lui, and H. Zeng, "Effect of formalin fixation on the near-infrared Raman spectroscopy of normal and cancerous human bronchial tissues," Int. J. Oncol. **23**, 649–655 (2003).